Stephanie L. Castro*, Sheila G. Bailey, Ryne P. Raffaelle, Kulbinder K. Banger and Aloysius F. Hepp
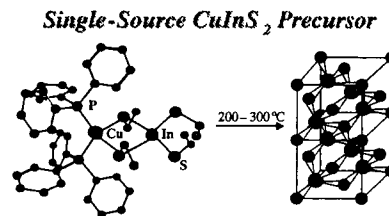
Nanocrystalline Chalcopyrite Materials (CuInS$_2$ and CuInSe$_2$) via Low-Temperature Pyrolysis of Molecular Single-Source Precursors.

Pyrolysis of ternary molecular single-source precursors in non-coordinating solvents yields nanocrystalline chalcopyrite materials. The precursors decompose at 200 °C to form an intermediate material, which forms CuInE$_2$ (E = S, Se) upon heating to 300 °C. The nanoparticles are probed by powder X-ray diffraction, absorption spectroscopy, and electron microscopy.

Single-Source CuInS$_2$ Precursor

Nanocrystalline Chalcopyrite Materials ($CuInS_2$ and $CuInSe_2$) via Low-Temperature Pyrolysis of Molecular Single-Source Precursors.

Stephanie L. Castro[*,1], Sheila G. Bailey[2], Ryne P. Raffaelle[3], Kulbinder K. Banger[1] and Aloysius F. Hepp[2]

1) Ohio Aerospace Institute, Cleveland, OH 44142; 2) Photovoltaics and Space Environments Branch, NASA Glenn Research Center, Cleveland, OH 44135; 3) Department of Physics, Rochester Institute of Technology, Rochester, NY 14623.

Abstract.   Nanometer sized particles of the chalcopyrite compounds $CuInS_2$ and $CuInSe_2$ were synthesized by thermal decomposition of molecular single-source precursors $(PPh_3)_2CuIn(SEt)_4$ and $(PPh_3)_2CuIn(SePh)_4$, respectively, in the non-coordinating solvent dioctyl phthalate at temperatures between 200 and 300 °C. The nanoparticles range in size from 3 – 30 nm and are aggregated to form roughly spherical clusters of about 500 nm in diameter. X-ray diffraction of the nanoparticle powders shows greatly broadened lines indicative of very small particle sizes, which is confirmed by TEM. Peaks present in the XRD can be indexed to reference patterns for the respective chalcopyrite compounds. Optical spectroscopy and elemental analysis by energy dispersive spectroscopy support the identification of the nanoparticles as chalcopyrites.

Keywords: chalcopyrite, nanocrystal, single-source precursor

Introduction. The space photovoltaic community is well aware of the cost benefits to both mission and spacecraft development associated with the continued increase in solar cell efficiency. The developmental efforts in regard to both Si- and GaAs-based cells have resulted in nearly eliminating the efficiency differences between actual devices and theoretical estimates. Over the past decade much of the cell efficiency improvements have resulted from the move towards multi-junction devices. However, as researchers continue to push the envelope, they are looking towards new approaches, such as the use of nanotechnology, in improving device performance.

Future photovoltaic devices may employ materials such as semiconductor quantum dots. The inclusion of nanocrystalline materials in photovoltaic devices[1] has been proposed as a means to improve the efficiency of photon conversion (intermediate band solar cell),[2,3,4] enable low-cost deposition of thin-films,[5] provide sites for exciton dissociation and pathways for electron transport.[6,7,8,9,10,11]

The Intermediate Band Solar Cell (IBSC) was proposed by Luque and Martí several years ago[2] as a means to greatly exceed the Schockley-Queisser efficiency of a cell. Their calculations predict a theoretical efficiency of over 63%, well in excess of the most efficient cells available today. The IBSC comprises a layer of size-graded quantum dots encapsulated in a barrier semiconductor, sandwiched between the p and n junctions of a solar cell. In their proposal,[2b] Stranski-Krastanow grown dots (InGaAs/AlGaAs system) 4 nm diameter and spaced 10 nm apart will give the highest efficiency.

Composites of quantum dots and conductive organic polymers have been employed to overcome some of the limitations of charge transport efficiency due to low electron mobility in conjugated organic polymers. Huynh et al.[6b] blended CdSe nanorods (7 x 60 nm, 90 wt.%) with poly (3-

hexylthiophene) (P3HT) and built a device with a conversion efficiency of 1.7% at AM1.5. Arici et al.[7b] have studied the photovoltaic properties of $CuInS_2$/methanofullerene composites and fabricated a working device with a conversion efficiency of 0.09%. Composites of CdS and polyaniline[11] have been shown to increase the open circuit photovoltage and short circuit current of a multilayer device compared to devices without CdS nanoparticles.

Quantum dots are also more resistant to degradation from electron, proton, and alpha particle radiation than the corresponding bulk material, preferred characteristics for use in space solar cells.[12,13,14] An InP p-i-n solar cell with quantum wells of InAsP has been shown to have greater resistance to proton irradiation than an InP cell without quantum wells included.[13] Another study[14] compared GaAs bulk structures to GaAs structures which contained InAs quantum dots or quantum wells. The structures containing quantum dots were found to be more resistant to electron radiation than those containing the quantum wells, which in turn were more resistant than the base GaAs structure. In these samples the quantum dots or wells were grown by MOCVD.

Chalcopyrite-based photovoltaic devices (Cu(In:Ga)(S:Se)$_2$) have been a focus of the space photovoltaic community for over two decades.[15,16,17] Thin-film photovoltaic devices made with the chalcopyrite semiconductors are expected to be highly efficient. Thin-film $CuInS_2$ cells with efficiencies of 12.5% have been successfully produced,[18] while efficiencies up to 18.8% have been recorded with Cu(In, Ga)Se$_2$-based cells.[19] The band gap of $CuInS_2$ (Eg = 1.5 eV) is well suited to the AM0 solar spectrum for photovoltaic performance. Although $CuInSe_2$ (Eg = 1.1 eV) is not as well suited, it has other attributes such as a high absorption coefficient and low-cost methods for deposition of thin-films which make $CuInSe_2$ a promising material for photovoltaic devices.

The possibility of increased efficiency and resistance to radiation-induced defects lead us to investigate quantum dots as part of our ongoing research on chalcopyrite materials for space photovoltaic applications. In contrast to the overall quantity of quantum dot research[20] in the literature, relatively few reports[21,22,23,24,25,26,27,28,29] have been published about the synthesis of nano-sized I-III-VI$_2$ ternary materials CuInS$_2$ and CuInSe$_2$.

O'Brien and co-workers[21] reported the synthesis of CuInSe$_2$ nanoparticles by the reaction of CuCl, InCl$_3$ and TOPSe in a TOP/TOPO mixture to form nearly spherical crystals with a diameter of approximately 4 nm. Czekelius et al.[22] reported the formation of 7 nm elongated nanocrystallites of CuInS$_2$ by treatment of a Cu^I-P(OPh)$_3$/In^{III}-P(OPh)$_3$ mixture in acetonitrile with (TMS)$_2$S. Gurin[23] reported the formation of nanocrystals of CuInS$_2$ or CuInSe$_2$ by treatment of an aqueous mixture of CuCl and In$_2$(SO$_4$)$_3$ with hydrogen sulfide or hydrogen selenide, respectively. In each case, the authors observed blue shifts of the absorption onset of the material with respect to the bulk values, indicative of size-induced quantum confinement. Qian and coworkers[24,27,28] have reported a series of solvothermal routes to non-colloidal nanoparticles of CuInS$_2$ and CuInSe$_2$, which have been characterized primarily by X-ray diffraction (XRD), transmission electron microscopy (TEM), and elemental analysis.

In practice however, synthesis of a desired size nanoparticle is not always simple. This is especially true for the higher-order ternary and tertiary materials. If separate sources are used for the different metals and chalcogenides, binary materials can be preferentially formed as a result of different solubility of the products and reactivity of the precursors.

A method to circumvent the formation of undesirable reaction products is through the use of single-source precursors. Single-source precursors are discrete molecules which include all the elements required in the final material. These precursors can be designed with many properties

in mind, including: stoichiometry, solubility, and volatility. As $CuInS_2$ is a promising material for thin-film photovoltaics and quantum dot solar cells, our group has studied the synthesis of potential precursors to $CuInS_2$ and $CuInSe_2$, and the subsequent conversion of these precursors to thin-films of the bulk semiconducting materials. [30,31,32,33] The molecular precursor $(PPh_3)_2CuIn(SEt)_4$ (Figure 1) was first described by Hirpo et. al. in 1993.[34] This charge-neutral molecule comprises a copper(I) ion bound by two triphenylphosphine ligands, an indium(III) ion with two terminal ethanethiolate ligands, and two bridging ethanethiolate ligands which coordinate in a μ_2- fashion between the metal centers. This molecule was found to decompose to $CuInS_2$ below 260 °C.
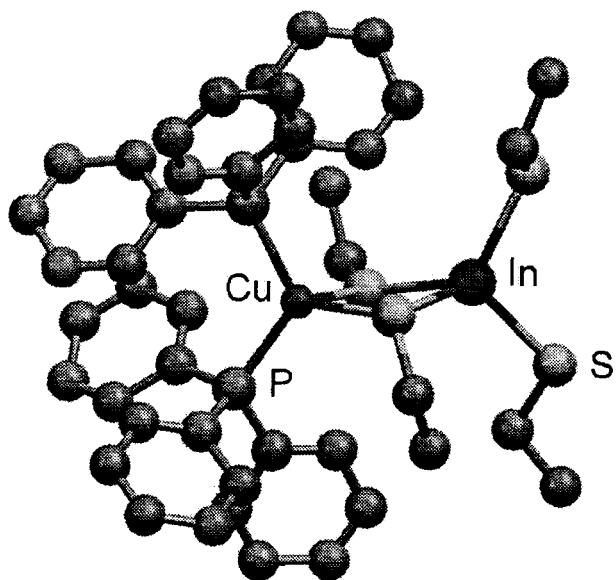

Figure 1. Molecular structure of $(PPh_3)_2CuIn(SEt)_4$

Further work with this class of molecules has yielded analogous precursors with desirable properties such as lower melting points (including the liquid precursor $(P^nBu_3)_2CuIn(SEt)_4)$[30a] and higher solubility in organic solvents. In this work, the precursor $(PPh_3)_2CuIn(SEt)_4$ (**1**) was used in the synthesis of $CuInS_2$ nanoparticles. The analogous compound $(PPh_3)_2CuIn(SePh)_4$ (**1'**)

was used in the synthesis of $CuInSe_2$ nanoparticles. To the best of our knowledge, this paper presents the first reported use of a ternary single-source precursor to synthesize chalcopyrite nanoparticles.

Experimental Section

Materials. $(PPh_3)_2CuIn(SEt)_4$ (**1**) and $(PPh_3)_2CuIn(SePh)_4$ (**1'**) were prepared by literature methods.[30c] The starting materials are slightly air sensitive and are stored in an argon-filled inert atmosphere drybox (Vac Atmospheres) to prevent decomposition. Dioctyl phthalate (99+ %) was purchased from ACROS and used without further purification. Methanol (Optima grade) and toluene (HPLC grade) were purchased from Fisher Scientific and used without further purification.

Measurement. Optical spectra were recorded on a Perkin Elmer Lambda 19 spectrophotometer; samples were embedded on 3M brand Scotch Tape for analysis. Scanning electron microscopy (SEM) was performed on a Hitachi S3000N microscope operating at 25 kV; samples were prepared by dispersing a few milligrams of powder in methanol or toluene prior to dropping on an aluminum support (SPI) and allowing the solvent to evaporate. Elemental analyses were collected with an EDAX energy dispersive X-ray spectrometer operating at 25 kV. The results were quantitated by ZAF standardless correction. Transmission electron microscopy (TEM) was performed on a Philips CM200 operating at 200 kV in bright field mode. The digital image was collected on a Gatan Imaging Filter (GIF 1k x 1k). The magnification was calibrated using the Mag*i*cal TEM standard (http://www.emsdiasum.com/ems/calibration/magical.html). The TEM grids were Ted Pella 01881 lacey carbon; samples were prepared by dipping the grid into a milliliter of methanol containing suspended nanocrystalline powder and allowing the methanol to evaporate. Powder X-ray patterns were obtained on a Philips X'Pert diffractometer using Cu Kα

radiation, excited at 45 kV and 40 mA. The X-rays were collimated at the source with a 10 mm mask and divergence slit set at 1°, and at the detector with a 2 mm receiving slit and anti-scatter slit set to 1°.

Preparation of CuInS$_2$ Nanoparticles. Dioctyl phthalate (10 mL) was heated to 125 °C under vacuum for one hour to dry and degas the solvent; the flask was backfilled with argon and cooled to room temperature prior to adding the precursor. (PPh$_3$)$_2$CuIn(SEt)$_4$ (1.945 g, 2.0 mmol) was added to the reaction flask and heating resumed. At approximately 150 °C the precursor dissolved to form a transparent yellow solution; no further change was observed with time at this temperature. At this point the solution could be returned to room temperature without re-precipitation of the precursor. Upon increase of the temperature to 200 °C a red powder (product **2**) began to precipitate within a few minutes; a reaction time of two hours was employed to complete the precipitation and maximize the yield. After cooling to room temperature under argon, the reaction mixture was washed to remove any unreacted precursor and the red powder was isolated by centrifugation. The powder was washed consecutively with toluene and methanol to remove reaction by-products and any unreacted starting material and was dried under vacuum at 60 °C. The washing and centrifugation steps were carried out in ambient atmosphere. The product appeared to be only slightly air-sensitive at room temperature; a green tinge has been observed on the surface of the powder after several weeks in ambient lab atmosphere. 0.427 g of **2** was collected and stored in a glove box for future use.

A portion of the red powder (100 mg) was subsequently returned to a flask containing fresh dioctyl phthalate (10 mL), heated to higher temperatures, 250 or 300 °C, and held for one hour. When the temperature is 250 °C, a brown/black powder (product **3**) was obtained; at 300 °C the

resulting powder was black (product **4**). Each powder was washed and dried in the same manner before analysis.

Preparation of CuInSe$_2$ Nanoparticles. The same procedure as above was followed for the CuInSe$_2$ precursor, the exception being that the precursor dissolved in the dioctyl phthalate at 138 °C. (PPh$_3$)$_2$CuIn(SePh)$_4$ (1.951 g, 1.47 mmol) was dissolved in 10 mL dioctyl phthalate. A red powder (0.523 g, product **2'**) was collected after two hours heating at 200 °C. At 250 °C, the XRD pattern (Figure 2b) of the resulting selenium-containing powder still exhibited substantial splitting of the 112 line (vida infra); temperatures of 275 and 300 °C were employed for the second and third steps, giving products **3'** and **4'**, respectively.

Results

X-ray Diffraction. XRD (Figure 2) clearly shows that pure CuInS$_2$ is the product of the reaction at 250 and 300 °C, and CuInSe$_2$ at 275 and 300 °C. In every pattern, significant broadening of the diffraction lines is apparent; particle sizes of 2.8 and 7.4 nm were calculated by the Scherrer formula for **3** and **4**, and 4.4 and 9.8 nm for **3'** and **4'**, respectively.

The XRD patterns of **2** and **2'** exhibit unusual splitting of the (112) peaks into two peaks roughly centered about the expected (112) position; the remaining two index peaks (204/220) and (116/312) are in their expected positions. An explanation of this observation is presented in the Discussion section.
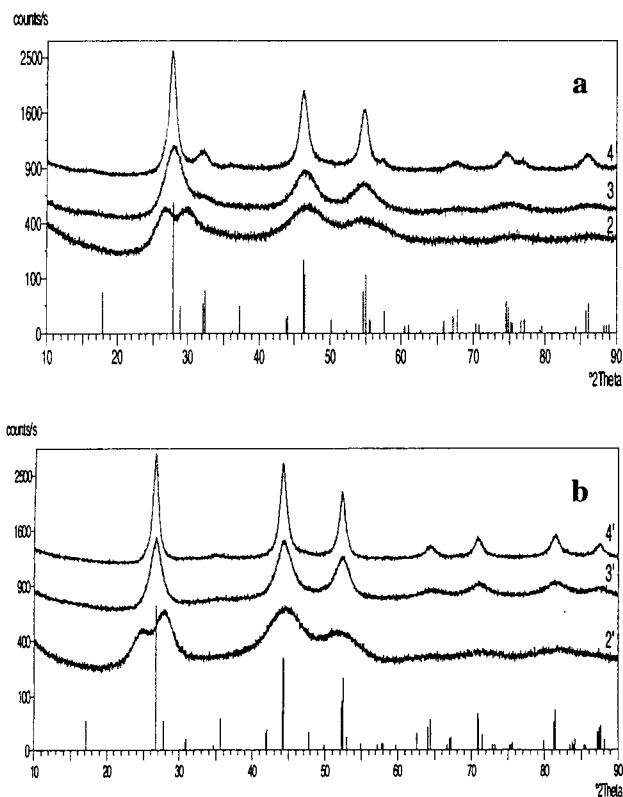
Figure 2. Powder XRD patterns for a) **2**, **3**, and **4**, the reaction products of (PPh₃)₂CuIn(SEt)₄ at 200, 250, and 300 °C, respectively. Reference pattern 85-1575 ($CuInS_2$) is shown along the x-axis; b) **2'**, **3'**, and **4'**, the reaction products of (PPh₃)₂CuIn(SePh)₄ at 200, 275, and 300 °C respectively. Reference pattern 87-2265 ($CuInSe_2$) is shown along the x-axis.

Optical Spectroscopy. Absorption spectroscopy of **2**, **3**, and **4** (Figure 3a and 3c) and **2'**, **3'** and **4'** (Figure 3b and 3d) immobilized on matte adhesive tape exhibited shifts of the absorption onsets relative to the $CuInS_2$ bulk band gap of 1.5 eV or $CuInSe_2$ at 1.1 eV. The absorbance onset of each product was determined by a least-squares fit of the linear region of a $(Ah\nu)^2$ vs. $h\nu$

plot (A = absorbance, h = Planck's constant, v = frequency).[35,36,37] The values for all products
are listed in Table 1.

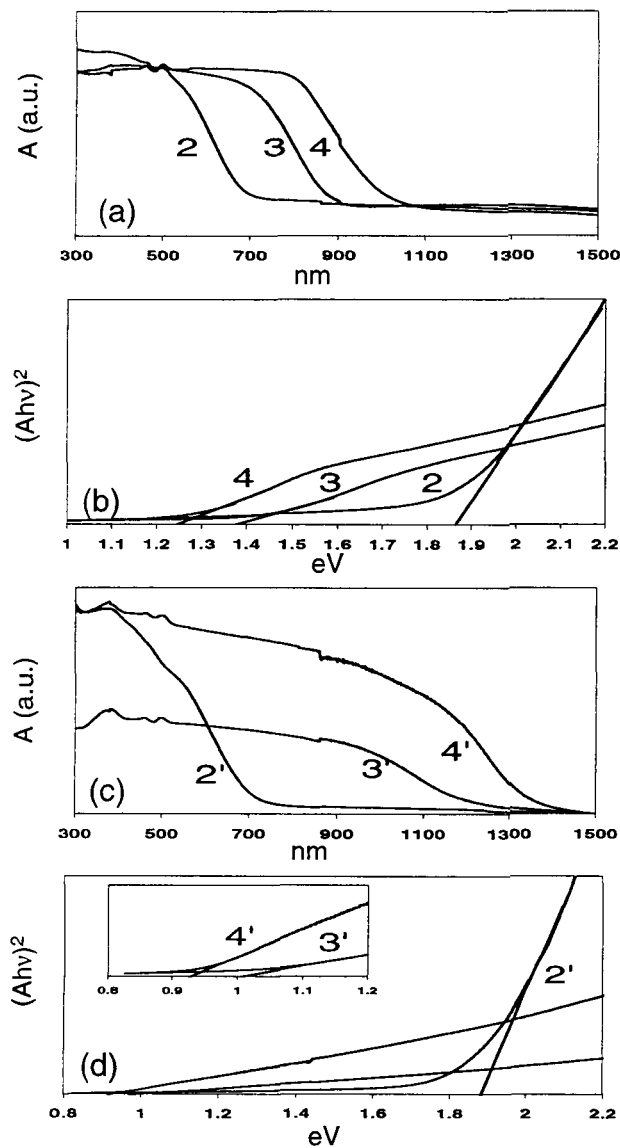Figure 3. a) Absorbance spectra of products **2**, **3**, and **4**; c) absorbance spectra of products **2'**, **3'**,
and **4'**; b) plots of $(Ahv)^2$ vs. energy for products **2**, **3** and **4**; d) plots of $(Ahv)^2$ vs. energy for
products **2'**, **3'**, and **4'**. Straight lines represent the least squares best fit to the linear region of the
plot; the inset in plot d shows the expanded region around the x-axis for products **3'** and **4'**.

Sample	Absorption Onset energy (eV)	Sample	Absorption Onset energy (eV)
2	1.86	**2'**	1.88
3	1.38	**3'**	1.01
4	1.25	**4'**	0.93

Table 1. Absorption onset energies for powdered samples immobilized on adhesive tape.

Electron Microscopy. The powders were examined by scanning and transmission electron microscopies. SEM (scanning electron microscopy) of all powders shows large spherical particles of ~500 nm diameter. Typical images are shown in Figure 4. At higher resolution, it was seen that the large particles are, in fact, aggregates of nanoparticles, as seen in Figure 5. From the HRTEM (high-resolution transmission electron microscopy) images, it appears that the size distribution of the samples is quite large, therefore, the sizes calculated by the Scherrer formula from the X-ray diffraction data are to be taken as averages.
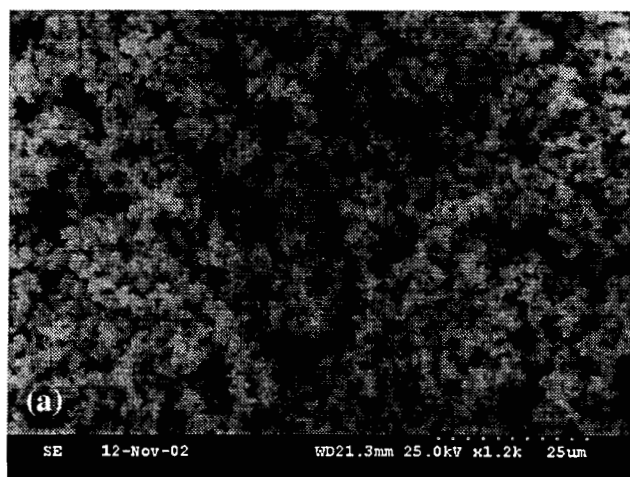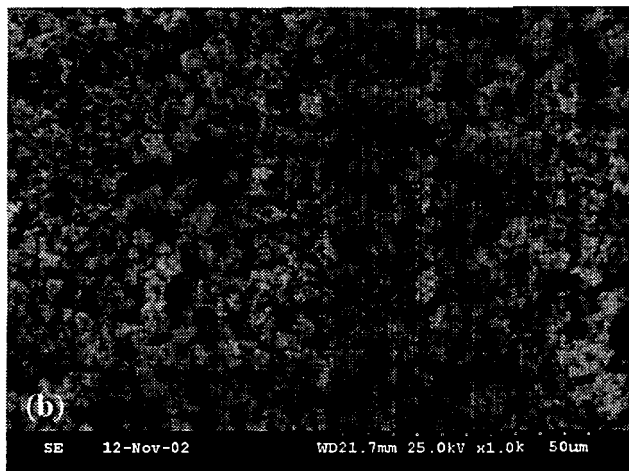
Figure 4. SEM images of a) **2** and b) **4**. Scale bars are 25 μm and 50 μm respectively.
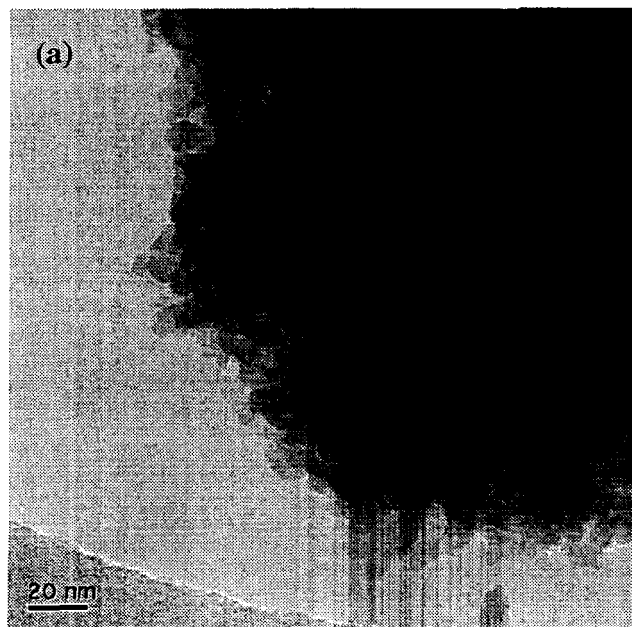
Figure 5. Medium (a) and high-resolution (b) TEM images of **4**. Scale bars are 20 nm and 5 nm respectively.

Discussion

Our initial research with this family of molecules stemmed from attempts to find a precursor for the chemical vapor deposition (CVD) of polycrystalline chalcopyrite films at temperatures compatible with lightweight substrates such as metal foils or polymers, which typically require deposition temperatures below 400 °C. Use of lightweight substrates is needed to optimize mass specific power and to minimize power system launch costs, both important considerations for space applications. Molecular design of CVD precursors is an important way to manipulate the volatility and decomposition temperature of the precursor, as well as to determine the purity of the film. While ternary single-source precursors should provide a very clean approach to the preparation of I-III-VI$_2$ materials, very few have been tested. In recent years, our group has

successfully exploited the flexible coordination chemistry of the copper and indium sites in this class of precursor molecules to exchange the indium atom for gallium, the thiolate for selenolate, and the phosphine Lewis base for arsines and stibines.[30b] The precursors have been used for the deposition of polycrystalline chalcopyrite films via spray CVD at 390 °C.

We have also recently begun investigating routes to nanocrystalline chalcopyrite materials. Based on our early success with the single-source precursors for chalcopyrite thin-films,[30-33] we have focused our efforts on the transformation of these molecules to chalcopyrite quantum dots. Initial attempts to use the "hot surfactant method" of colloidal nanoparticle synthesis failed. This method, pioneered by Murray et al in 1993,[38] involves injection of a precursor(s) dissolved in a solvent into a surfactant heated to ~300 °C. A persistent theme in the choice of surfactant is that it has metal-coordinating properties, although recent results from the Peng group show a possible avenue away from this restriction.[39] Injection of the $CuInS_2$ precursor into common coordinating solvents such as trioctylphosphine, oleic acid, stearic acid or hexadecylamine, or some combinations of these, lead to separation of the precursor components into binary materials such as copper sulfide. It is also possible that during dissolution in trioctylphosphine, the precursor loses its molecular integrity, with the phosphine solvent participating in the copper ligation and breaking apart the precursor. In the spray pyrolysis process for which the precursors were developed, the working solvent is toluene, and the precursors have good solubility without decomposition (at room temperature). For this reason, we then moved to a non-coordinating solvent. Dioctyl phthalate was chosen based on its boiling point (384 °C).

The precursors dissolved completely in dioctyl phthalate with moderate heating to form a yellow solution (the precursor in the solid state is white to yellowish white), and began to change to orange and red at 200 °C, followed immediately by precipitation. A disadvantage of a non-

coordinating solvent is that the solvent cannot act as a surfactant, binding to the surface of the growing nanocrystal and preventing aggregation with its neighbors. SEM and TEM showed the precipitate to be made up of large clusters of smaller nanocrystals. Future work includes post-processesing alteration of the surface of the nanoparticles to enable dispersion in solvents, and subsequent narrowing of the size distributions by size-selective precipitation.[38] A surfactant-passivated nanocrystal surface allows for controlled growth of colloidal nanocrystals.

The size of the nanoparticle is an important factor in determining the optoelectronic properties of the material. When the size of a semiconductor quantum dot drops below that of the exciton Bohr radius (of the bulk material) the energy levels become quantized and the band gap increases as the particle size decreases, resulting in a blue shift of the absorption onset energy. In this size regime the band gap can be "tuned" to a desired energy by adjusting the particle size, which offers the possibility of growing quantum dots to specifically match a portion of the solar spectrum. Many advances have been made in the last decade in synthetic control over colloidal nanoparticles, especially for the II-VI and III-V semiconductors.[40] Colloidal synthesis of quantum dots also offers greater control over the morphology and size of the dots than MOCVD methods, particularly for very small dots.

The stepwise method of synthesis, isolating the red intermediate before raising the temperature, was found to be critical for the purest products. If the precursor was brought directly to 250 or 300 °C, the final black powder was predominantly $CuInS_2$, but impurity peaks were evident in the XRD pattern. The reactions are outlined in Scheme 1. It was hypothesized that the red material could be an intermediate precursor comprising a mixture of Cu_xE_y and In_xE_y (E = S or Se) which could recombine at higher temperatures to form $CuInE_2$. An extensive search of the JCPDS-ICDD XRD database, focusing especially on the binary and ternary mixtures of Cu, In,

and S or Se found no clear matches to known phases which incorporated all the features observed in the experimental patterns while omitting no major peaks from the reference pattern. In addition, it is well established that covellite (CuS, more accurately represented as the mixed-valence compound $Cu^I_4Cu^{II}_2(S_2)_2S_2$[41]) is dissolved by aqueous KCN solutions. In a 2002 study of the etching effects of KCN on CuS contaminated $CuInS_2$, Weber et al.[42] studied the selective dissolution of CuS from the surface of a chalcopyrite sample. They determined that a 1% aqueous KCN solution dissolved CuS at a rate of 5-10 nm/sec. A 100 mg sample of the red powder was washed with for two ten minute periods with gentle agitation. On the basis of the previous study, ten minutes would be sufficient to dissolve up to six micron diameter particles. The sample was washed thoroughly with distilled water and dried under vacuum. The XRD pattern of the product was completely unaffected by the KCN wash. From this it is possible to conclude that copper sulfide, with the copper in either the mono- or divalent state, is not a significant component of **2**. It is not possible to assign the identity of **2** and **2'** on the basis of XRD patterns. Investigation into the identity of these materials is on-going. It is important to note though, that identification of these products is not critical to this report, as both **2** and **2'** are cleanly converted to the desired chalcopyrite materials at higher reaction temperatures (250 and 275 °C, respectively).

Optical spectroscopy was also employed to characterize the nanocrystals. An increase in band-gap energy is one of the characteristics of size-quantization in semiconductor nanoparticles. However, the absorption onsets for **3, 4, 3'** and **4'** are at lower energy than those of the bulk band-gaps. The onset for **3** is ~1.38 eV, and **4** is ~1.2 eV. Sub-band-gap absorption is not uncommon for $CuInE_2$ (E = S, Se); it has been observed in thin-films and polycrystalline samples. It can be attributed to surface defects and grain boundaries. In theory, both of these

should diminish in importance with increasing sample preparation temperature, as the particles should both increase in size and defects at the surface should anneal out. The apparent opposite is observed here, the onset of absorption for **4** (prepared at 300 °C) shows a sub-band-gap absorption at even lower energy than for **3** (prepared at 250 °C). The same trend is observed for the $CuInSe_2$ powders, see Figure 3b and 3d. These observations are likely due to the relatively low synthesis temperatures compared to the typical bulk annealing temperatures at 600-700 °C.

Elemental analysis by ZAF standardless correction (Table 2) of the powders by EDS (energy dispersive spectroscopy) shows Cu:In:S(Se) ratios close to those expected for the products.

Sample	Cu	In	S (Se)
2	1.0	0.91	2.28
3	1.0	0.89	1.58
4	1.0	0.94	1.83
2'	1.0	1.18	(3.09)
3'	1.0	1.11	(2.19)
4'	1.0	1.03	(2.27)

Table 2. Elemental ratio in products determined by EDS.

Conclusion

The CVD precursors $(PPh_3)_2CuIn(SEt)_4$ and $(PPh_3)_2CuIn(SePh)_4$ can be converted to nanocrystalline chalcopyrite materials $CuInS_2$ and $CuInSe_2$, respectively, by thermolysis in a non-coordinating solvent. The conversion takes place in two steps: first by formation of an as-yet unidentified red intermediate, followed by further transformation to the chalcopyrite structure.

The identity of the material is confirmed by powder x-ray diffraction; evidence of the nanometer-scale particle diameters is confirmed by TEM. The average size of the nanoparticles as determined by TEM, as well as the lack of a blue shift in the absorption energy of products **3, 4, 3'** and **4'** indicates that the particles are likely not small enough to exhibit size quantization effects, and, while nanoparticles, are not truly "quantum dots". The Bohr exciton radii[43] of $CuInS_2$ and $CuInSe_2$ are 4.1 and 10.6 nm, respectively. The material is largely aggregated, however we are optimistic that these precursors may still provide a route to colloidal chalcopyrite quantum dots.

* Corresponding author: Stephanie Castro. c/o NASA Glenn Research Center, Mail Stop 302-1, 21000 Brookpark Rd. Cleveland, OH 44135. E-mail: stephanie.castro@grc.nasa.gov.

[1] A collection of reviews on this topic is available in a special issue of *Physica E* (**2002**, *14*, issue 1-2) entitled "Nanostructures in Photovoltaics".

[2] a) Luque, A. and Martí, A. *Phys. Rev. Lett.* **1997**, *78*, 5014 – 5017; b) Martí, A.; Cuadra, L. and Luque, A. "Quantum Dot Intermediate Band Solar Cell" In *Twenty-eighth IEEE Proceedings of the Photovoltaics Specialists Conference*, Anchorage, Alaska, September 2000, IEEE: 2000, pp. 940 – 943.

[3] Aroutiounian, V.; Petrosyan, S.; Khachatryan, A. and Touryan, K. *J. Appl. Phys.* **2001**, *89*, 2268 – 2271.

[4] Raffaelle, R. P.; Castro, S. L.; Hepp, A. F. and Bailey, S. G. *Prog. Photovolt. Res. Appl.* **2002**, *10*, 433 – 439.

[5] Eberspacher, C.; Pauls, K. L. and Fredric, C. V. "Improved Processes for Forming $CuInSe_2$ Films" In *Twenty-ninth IEEE Proceedings of the Photovoltaics Specialists Conference*, New Orleans, Louisiana, May 2002, IEEE: 2002.

[6] a) Huynh, W. U.; Peng, X. and Alivisatos, A. P. *Adv. Mater.* **1999**, *11*, 923 - 927; b) Huynh, W. U.; Dittmer, J. J. and Alivisatos, A. P. *Science* **2002**, *295*, 2425 - 2427.

[7] a) Arici, E.; Hoppe, H.; Reuning, A.; Sariciftci, N. S. and Meissner, D. "CIS Plastic Solar Cells" in *Seventeenth European Photovoltaic Solar Energy Conference Proceedings*, Munich, Germany 2001, James and James Ltd, London, 2001; b) Arici, E.; Sariciftci, N. S. and Meissner, D. *Mol. Cryst. Liq. Cryst.* **2002**, *385*, 249 – 256.

[8] Grätzel, M. *Prog. Photovolt.: Res. Appl.* **2000**, *8*, 171 – 185.

[9] Wang, Y. and Herron, N. *J. Lumin.* **1996**, *70*, 48 – 59.

[10] Nozik, A. J. *Ann. Rev. Phys. Chem.* **2001**, *52*, 193 – 231.

[11] a) Godovsky, D. Y.; Varfolomeev, A. E.; Zaretsky, D. F.; Chandrakanthi, R. L. N.; Kündig, A.; Weder, C. and Caseri, W. *J. Mater. Chem.* **2001**, *11*, 2465 – 2469; b) Chandrakanthi, R. L. N. and Careem, M. A. *Thin Solid Films* **2002**, *417*, 51 – 56.

[12] Marcinkevičius, S.; Leon, R.; Čechavičius, B.; Siegert, J.; Lobo, C.; Magness, B. and Taylor, W. *Physica B* **2002**, *314*, 203 – 206.

[13] Walters R. J.; Summers, G. P.; Messenger, S. R.; Freundlich, A.; Monier, C. and Newman, F. *Prog. Photovolt: Res. Appl.* **2000**, *8*, 349 – 354.

[14] Sobolev, N. A.; Cavaco, A.; Carmo, M. C.; Grundmann, M.; Heinrichsdorff, F. and Bimberg, D. *Phys. Stat. Sol B* **2001**, *224*, 93 – 96.

[15] Bailey, S. G. and Flood, D. J. *Prog. Photovolt. Res. Appl.* **1998**, *6*, 1 – 14.

[16] Schock, H. W. and Noufi, R. *Prog. Photovolt. Res. Appl.* **2000**, *8*, 151 – 160.

[17] Schock, H. W. and Bogus, K. "Development of CIS solar cells for space applications" in *Proceedings of the Second World Conference on Photovoltaic Energy*, Schmid, J.; Ossenbrink, H. A.; Helm, P.; Ehmann, H, and Dunlop, E. D. (eds) EC Joint Research Center, Luxembourg, 1998, 3586 – 3589.

[18] Klaer, J.; Bruns, J.; Henninger, R.; Töpper, K.; Klenk, R.; Ellmer, K. and Bräunig, D. in *Proceedings of the Second World conference on Photovoltaic Solar Energy Conversion*, Schmid, J.; Ossenbrink, H. A.; Helm, P.; Ehmann, H, and Dunlop, E. D. (eds) EC Joint Research Center, Luxembourg, July 1998, 537 – 540.

[19] Contreras, M. A.; Egaas, B.; Ramanathan, K.; Hiltner, J.; Swartzlander, A.; Hasoon, F. and Noufi, R. *Prog. Photovolt.: Res. Appl.* **1999**, *7*, 311 – 316.

[20] A search of the term "quantum dot*" in the Science Citation Index in March, 2003 yielded 10,800 hits.

[21] Malik, M. A.; O'Brien, P. and Revaprasadu, N. *Adv. Mater.* **1999**, *11*, 1441 – 1444.

[22] Czekelius, C.; Hilgendorff, M.; Spanhel, L.; Bedja, I.; Lerch, M.; Müller, G.; Bloeck, U.; Su, D.-S. and Giersig, M. *Adv. Mater.* **1999**, *11*, 643 – 646.

[23] Gurin, V. S. *Coll. Surf. A* **1998**, *142*, 35 – 40.

[24] a) Lu, Q.; Hu, J.; Tang, K.; Qian, Y.; Zhou, G. and Liu, X. *Inorg. Chem.* **2000**, *39*, 1606 – 1607; b) Cui, Y.; Ren, J.; Chen, G.; Qian, Y. and Xie, Y. *Chem. Lett.* **2001**, 236 – 237; c) Jiang, Y.; Wu, Y.; Yuan, S.; Xie, B.; Zhang, S. and Qian, Y. *J. Mater. Res.* **2001**, *16*, 2805 – 2809.

[25] Gurinovich, L. I.; Gurin, V. S.; Ivanov, V. A.; Bodnar, I. V.; Molochko, A. P. and Solovej, N. P. *phys. stat. sol. b* **1998**, *208*, 533 – 540.

[26] Malyarevich, A. M.; Yumashev, K. V.; Posnov, N. N.; Mikhailov, V. P.; Gurin, V. S.; Prokopenko, V. B.; Alexeenko, A. A. and Melnichenko, I. M. *J. Appl. Phys.* **2000**, *87*, 212 – 216.

[27] Jiang, Y.; Wu, Y.; Mo, X.; Yu, W.; Xie, Y. and Qian, Y. *Inorg. Chem.* **2000**, *39*, 2964 – 2965.

[28] a) Xiao, J.; Xie, Y.; Tang, R. and Qian, Y. *J. Mater. Chem.* **2001**, *11*, 1417 – 1420; b) Xiao, J.; Xie, Y.; Tang, R. and Qian, Y. *J. Sol. St. Chem.* **2001**, *161*, 179 – 183; c) Li, B.; Xie, Y.; Huang, J. and Qian, Y. *Adv. Mater.* **1999**, *11*, 1456 – 1459.

[29] Mandale, A. B.; Sathaye, S. D. and Patil, K. R. *Mater. Lett.* **2002**, 55, 30 – 33.

[30] a) Banger, K. K.; Cowen, J. and Hepp, A. F. *Chem. Mater.* **2001**, *13*, 3827 – 3829; b) Banger, K. K.; Harris, J. D.; Cowen, J. E. and Hepp, A. F. *Thin Solid Films* **2002**, *403-404*, 390 – 395; c) Banger, K. K.; Hollingsworth, J. A.; Harris, J. D.; Cowen, J.; Buhro, W. E. and Hepp, A. F. *Appl. Organomet. Chem.* **2002**, *16*, 617 – 627.

[31] Henderson, D. O.; Mu, R.; Ueda, A.; Wu, M. H.; Gordon, E. M.; Tung, Y. S.; Huang, M.; Keay, J.; Feldman, L. C.; Hollingsworth, J. A.; Buhro, W. E.; Harris, J. D.; Hepp, A. F. and Raffaelle, R. P. *Mater. Des.* **2001**, *22*, 585 – 589.

[32] Raffaelle, R. P.; Potdevin, T.; Hepp, A. F. and Bailey, S. G. *Mater. Sci., Semicon. Proc.* **1999**, *2*, 289 – 296.

[33] Hollingsworth, J. A.; Hepp, A. F. and Buhro, W. E. *Chem. Vap. Dep.* **1999**, *5*, 105 – 109.

[34] Hirpo, W.; Dhingra, S.; Sutorik, A. C. and Kanatzidis, M. G. *J. Am. Chem. Soc.* **1993**, *115*, 1597 – 1599.

[35] Onnagawa, H.; Miyashita, K. *Jap. J. Appl. Phys.* **1984**, *23*, 965 – 969.

[36] Shay and Wernick, *Ternary Chalcopyrite Semiconductors* Pergamon, Oxford, **1975** p. 118.

[37] Rajaram, R.; Thangaraj, R.; Sharma, A. K.; Raza, A. and Agnihotri, O. P. *Thin Solid Films* **1983**, *100*, 111 – 116.

[38] Murray, C. B.; Norris, D. J.; and Bawendi, M. G. *J. Am. Chem. Soc.* **1993**, *115*, 8706 – 8715.

[39] Yu, W. W. and Peng, X. *Angew. Chem. Int. Ed.* **2002**, *41*, 2368 – 2371.

[40] For reviews of this topic see: Murray, C. B.; Kagan, C. R. and Bawendi, M. G. *Annu. Rev. Mater. Sci.* **2000**, *30*, 545 - 610 and Trindade, T.; O'Brien, P. and Pickett, N. L. *Chem. Mater.* **2001**, *13*, 3843 – 3858.

[41] Robbins, M.; Bachmann, K. J.; Lambrecht, V. G.; Thiel, F. A.; Thomson, J.; Vadimsky, R. G.; Menezes, S.; Heller, A. and Miller, B. *J. Electrochem. Soc.* **1978**, *125*, 831 – 832.

[42] Weber, M.; Scheer, R.; Lewerenz, H. J.; Jungblut, H. and Störkel, U. *J. Electrochem. Soc.* **2002**, *149*, G77 – G84.

[43] The Bohr exciton radius is calculated by $r_B = \dfrac{\varepsilon_{dot}}{\mu} a_B$, where $\mu = \dfrac{1}{m_e^{*-1} + m_h^{*-1}}$, a_B is the hydrogen Bohr radius, ε_{dot} is the dielectric constant of the bulk material, and m_e^* and m_h^* are the reduced masses of the electron and hole. Values for $CuInS_2$ ($m_e^* = 0.16$, $m_h^* = 1.3$, $\varepsilon_{dot} = 11$) and $CuInSe_2$ ($m_e^* = 0.82$, $m_h^* = 0.71$ and $\varepsilon_{dot} = 14.7 \pm 1.3$) were obtained from references 22 and 44, respectively.

[44] Rincón, C.; Márques, R. *J. Phys. Chem. Sol.* **1999**, *60*, 1865 – 1873.